

Electron localization in (7×7) reconstructed and hydrogen-covered Si(111) surfaces as seen by NMR on adsorbed Li

H. Winnefeld,¹ M. Czanta,² G. Fahsold,³ H. J. Jänsch,¹ G. Kirchner,¹ W. Mannstadt,¹ J. J. Paggel,^{1,*} R. Platzer,¹ R. Schillinger,² R. Veith,¹ C. Weindel,¹ and D. Fick¹

¹Philippis-Universität, Fachbereich Physik und Zentrum für Materialwissenschaften, D-35032 Marburg, Germany

²Max-Planck-Institut für Kernphysik, D-69029 Heidelberg, Germany

³Universität Heidelberg, Kirchoff-Institut für Physik, D-69120 Heidelberg, Germany

(Received 20 December 2001; published 10 May 2002)

The observation of “Korringa-like” nuclear-spin-lattice relaxation of ^8Li probe atoms, adsorbed at extremely low coverages on the Si(111)- (7×7) surface (10^{-4} ML and below) points to the existence of a correlated two-dimensional electron gas. The observed high relaxation rates as compared to adsorption of ^8Li on metals are in accordance with an enhanced electron localization in the adatom dangling bonds. For ^8Li adsorbed on semiconducting hydrogen covered Si(111) surfaces (now at coverages around 10^{-3} ML) “Korringa-like” spin-lattice relaxation is also observed, quite surprisingly. Independent of the preparation of the hydrogen coverage, i.e., in vacuum or wet chemically terminated, the relaxation rates are moreover all of the same size. This points to a narrow band at the Fermi energy generated by the adsorbed Li itself. Quantitative *ab initio* all-electron density-functional calculations for Li coverage as low as 0.04 on the perfectly hydrogen-terminated Si(111) surface together with a qualitative reasoning following Mott’s arguments on semiconductor-metal transitions support this view.

DOI: 10.1103/PhysRevB.65.195319

PACS number(s): 73.20.Hb, 76.60.-k, 76.30.-v

I. INTRODUCTION

Due to its dangling bonds the (7×7) reconstruction of the Si(111) surface contains many hallmarks of a metallic surface. Recently, not only has a parabolic dispersive band located at the center of the (7×7) Brillouin zone been identified,¹ but also “Korringa-like nuclear-spin relaxation” was observed in NMR experiments on Li, adsorbed at extremely low coverages of 10^{-4} monolayer (ML) and below,² which is on average only one Li atom per 200 unit cells of the (7×7) reconstruction. Nuclear-spin-lattice relaxation rates, henceforth denoted as $\alpha=1/T_1$, describe the rate of change of the nuclear polarization (magnetization) with time towards thermal equilibrium. In classical NMR experiments,³⁻⁵ T_1 denotes the built-up time; here it denotes the polarization decay time, since the initial value is far above the thermal equilibrium value (see Sec. II).

Relying on common wisdom, the observation of “Korringa-like” nuclear-spin relaxation, magnetic-field-independent relaxation rates linear in temperature, is considered an unequivocal sign of the “metallicity” of a system.³⁻⁶ In what follows, we will be more careful and consider it a sign of an at least partly delocalized electron gas with correlation times much shorter than the electron Larmor period for the magnetic field used (for details, see Sec. III).

In contrast to the clean (7×7) surface, the hydrogen-covered Si(111):H surface has saturated dangling bonds and is semiconducting, the latter proven experimentally⁷⁻¹⁰ as well as theoretically.¹¹⁻¹⁴ (See also Fig. 5 below in Sec. IV.) However, surprisingly enough, in NMR experiments on adsorbed Li “Korringa-like” nuclear-spin relaxation was observed as well.² This points to fluctuating electromagnetic fields with correlation times much shorter than the nuclear Larmor period in the external magnetic field. (For details see

the end of Sec. III.) From where could these fluctuations arise? The dipole-dipole interaction of the proton magnetic moments of the adsorbed hydrogen atoms with the adsorbed Li nuclear magnetic moments is too weak. Moreover, as argued in more detail previously, the relaxation rate should decrease rather than increase with temperature.² Therefore, the interaction which causes the fluctuations is more likely of electronic origin. Here, paramagnetic centers may be considered, since *in situ* hydrogen-covered surfaces are not as perfect as assumed in theoretical calculations. For one of the preparation methods used (called “cold” hydrogen adsorption below) one finds with scanning tunneling microscopy (STM) for a saturated surface still isolated adatoms at small islands, which are made up of the missing adatoms from the exposed region of the rest layer.⁸ But, again, if paramagnetic centers cause magnetic-field-independent spin-lattice relaxation rates, they will decrease rather than increase with temperature as observed in the experiment.²

Previously, the experiments have been performed with *in situ* “cold” hydrogen-covered Si(111):H surfaces only.² Higher quality surfaces, denoted henceforth as “hot” hydrogen-covered Si(111):H ones, are obtained by adsorbing hydrogen *in situ* at elevated temperatures around 400 °C to 500 °C and strongly increased H/H₂ partial pressure.^{15,16} But the best hydrogen-covered surfaces are obtained through wet chemical etching (hydrogen termination).^{17,18} The use of the latter technique requires, however, a kind of “clean room” and a fast load lock to transfer the “as-prepared surfaces” into the UHV. Moreover, annealing this wet chemically hydrogen terminated Si(111)-(1 \times 1):H surface seems to be crucial in the NMR experiments, since due to passivation through hydrogen, one deals without always annealing with an undoped surface with midgap Fermi energy.¹⁹⁻²² For such prepared surfaces, “Korringa-like” relaxation should disappear.

It was one of the main purpose of the present experiment to test whether “Korringa-like” relaxation prevails in NMR experiments on Li adsorbed on hot hydrogen-covered and, most importantly, annealed wet chemically hydrogen-terminated Si(111) surfaces (Sec. IV). To this end, as compared to an experiment described in a recent publication,² more extended experiments on the clean surface will be used as a reference level (Sec. III). Moreover, a more sophisticated interpretation of the large relaxation rates found in the previous experiment will be presented. The experimental setup, in particular the part which enables us to use wet chemically hydrogen-terminated Si(111)-(1×1):H surfaces in the environment of a purely nuclear-physics-based accelerator laboratory, is described in Sec. II. The paper closes with an outlook in Sec. V.

II. THE EXPERIMENT

Except for the preparation of the hydrogen-covered and -terminated surfaces, this experiment has been performed with the same technique as described recently.² We therefore describe this part of the experiment only briefly.

The UHV chamber used has a base pressure of 3×10^{-11} mbar. It is equipped with conventional low-energy electron-diffraction (LEED) optics, an Auger electron spectrometer (AES), a mass spectrometer, leak valves for gas dosing, and a commercial Kelvin probe for work-function measurements. “Temperature programmed desorption” (TPD) spectroscopy is used as well.

The chamber is connected to a homemade load lock, built mainly for a fast transfer of wet chemically prepared hydrogen-terminated Si(111)-(1×1):H surfaces (see Appendix A). The Si samples are transferred in a small Mo shuttle. The construction allows for indirect heating of the sample by electron bombardment and cooling with liquid N₂. Most of the construction is made from low H₂ and unmagnetic steel (1.4429 esu) to avoid any kind of stray magnetic fields during NMR experiments. After feeding the load lock with the sample it takes about four minutes to reach 5×10^{-8} mbar and after opening the valve to the UHV chamber another seven minutes until the sample is in an UHV environment of 3×10^{-11} mbar.

The clean (7×7) reconstructed samples from modestly *n*(P)- and *p*(B)-doped wafers were prepared in the standard way as described in more detail in Ref. 2. Hydrogen-covered Si(111):H samples were prepared by two *in situ* techniques, both adsorbing atomic H, either onto a “cold”^{8,23} or “hot”^{15,16,24} Si(111)-(7×7) surface and hydrogen-terminated Si(111)-(1×1):H ones by Chabal *et al.*’s *ex situ* “wet” chemical technique of hydrogen termination.²⁵ Aside from LEED patterns and AES spectra TPD experiments were mainly used to characterize the hydrogen-covered and -terminated surfaces. Additionally, infrared transmission spectroscopy (IRTS) and an atomic force microscope (AFM) were applied to characterize the hydrogen-terminated surfaces further. Even though highly desirable, STM could not be applied because of the already mentioned hostile and strongly vibrating environment of an accelerator

laboratory. Details of the sample preparation are summarized in Appendix A.

Another important but unusual instrument is the source providing a polarized ⁸Li atomic beam of thermal velocity.^{26,27} At the site of the sample it provides a thermal atomic beam of about 10⁸ lithium atoms/s (mainly ⁷Li), containing a small amount of about 10⁴ atoms/s of the nuclear-spin-polarized radioactive isotope ⁸Li (polarization $P = 0.8-0.9$). It is produced via the ²H(⁷Li,⁸Li) ¹H nuclear reaction by bombarding a deuterium gas target with 24-MeV ⁷Li³⁺ ions from the MP-tandem accelerator at the Max-Planck-Institute for Nuclear Physics in Heidelberg. The source can produce ⁸Li atoms (nuclear-spin $I=2$; magnetic dipole moment $\mu/\mu_N=1.65$, with μ_N the nuclear magneton) either in their $m=+2$ or $m=-2$ state (positive and negative polarization).

⁸Li is a β -decaying nucleus with a half-life of $T_{1/2} = 0.84$ s. Spin polarization of the adsorbate ⁸Li itself can therefore be detected via the directional asymmetry of the β decay. The asymmetry ϵ of the β -electron intensity with respect to the magnetic field is measured by scintillator telescopes (Fig. 1). The nuclear polarization P of the ⁸Li ensemble is determined from the observed asymmetry ϵ as

$$\epsilon = \frac{N(0^\circ) - N(180^\circ)}{N(0^\circ) + N(180^\circ)} = -\frac{1}{3}P. \quad (1)$$

Here $N(0^\circ)$ denotes the count rates for electrons emitted along the direction of the magnetic field, while $N(180^\circ)$ denotes the count rate for electrons emitted opposite to it. The factor $(-\frac{1}{3})$ is due to the nuclear properties of the ⁸Li β decay. Systematic errors in the determination of ϵ are eliminated by performing the experiment with the reverse polarization P as well. Details of the signal detection can be found in Refs. 28 and 29.

The nuclear-spin-relaxation experiments consist basically of three subsequent steps which are repeated many times. They start with a collecting period (typically 1.5 s) during which ⁸Li is produced and accumulated in the thermalizer.²⁷ Afterwards it is released while production is ongoing. An atomic beam is formed and nuclear-spin polarized by optical pumping. The thermal ⁸Li atoms are adsorbed on the surface for 0.5 s. Finally during the detection period of 4 s the β -electron asymmetry ϵ [Eq. (1)] is measured as a function of time. During the detection period the ion beam, the main source of background signals, is switched off. It is also possible to measure the asymmetry during the activation period properly taking into account the large background caused mainly by neutrons which are generated by nuclear reactions initiated by the 24-MeV ⁷Li beam. (See the “kink” in Fig. 2.)

Since ⁸Li possesses a nuclear-spin $I=2$ the decay of nuclear polarization with time can be expressed in general as the sum of four exponentials. (For details see Ref. 30 and Appendix A of Ref. 31.) However, in practice two exponentials at most were sufficient to describe the data. Figure 2 displays as a typical example $\epsilon(t)$ data for ⁸Li adsorption on a (“hot”) hydrogen-covered Si(111) surface kept at $T = 560$ K. Two exponentials are easily visible. The kink at

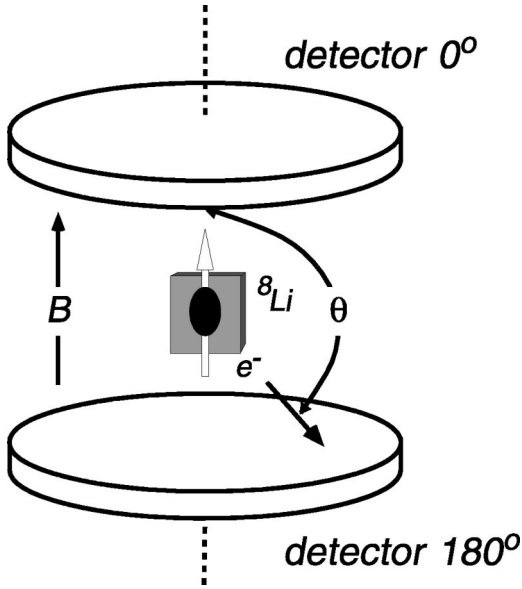


FIG. 1. The principle of β NMR: the decay electrons are emitted with a higher probability opposite to the direction of the nuclear spin. The normalized asymmetry ϵ of the count rates $N(0^\circ)$ and $N(180^\circ)$ yields the polarization of the spin ensemble.

$t=0$ is a consequence of the end of the activation period; from $t=0$ on, no new ^8Li is adsorbed on the surface. Parametrizing the asymmetry as

$$\epsilon(t) = \epsilon_0(q_{\text{fast}}e^{-\alpha_{\text{fast}}t} + q_{\text{slow}}e^{-\alpha_{\text{slow}}t}) \quad (2)$$

with $q_{\text{fast}} + q_{\text{slow}} = 1$, the data in Fig. 2 can be described by the relaxation rate $\alpha_{\text{fast}} = (16.0 \pm 3.8) \text{ s}^{-1}$ and $\alpha_{\text{slow}} = (0.63 \pm 0.09) \text{ s}^{-1}$, that is, $T_1^{\text{fast}} = 0.063 \text{ s}$ and $T_1^{\text{slow}} = 1.59 \text{ s}$, respectively. The initial asymmetry turned out to be $\epsilon_0 = (0.24 \pm 0.03)$, and the fast and slow fractions were $q_{\text{fast}} = 0.21$ and $q_{\text{slow}} = 0.79 \pm 0.03$, respectively.

From NMR experiments in semiconductors it is long known that the magnetization of dopants does not decay monoexponentially with time.^{32–34} This is usually attributed to the existence of delocalized and localized electrons. The latter contribute mainly to α_{fast} whereas the delocalized ones contribute mainly to α_{slow} .

It was not always possible to disentangle fast and slow relaxation as nicely as it was for the data of Fig. 2. However, the slow relaxation rate could always be determined accurately. We therefore mainly concentrate in this paper on $\alpha_{\text{slow}} \equiv \alpha = 1/T_1$ and postpone the discussion of the other variables, including the determination of ϵ_0 , to a forthcoming publication.

We close this section by remarking that contrary to conventional NMR experiments^{3–5} the determination of α or T_1 does not require the application of resonant rf fields. Since the nuclear-spin polarization P in thermal equilibrium is of the order of 10^{-5} , it can be neglected compared to the initial polarization of the ^8Li ensemble of 0.8 or 0.9.

III. THE Si(111)-(7×7) SURFACE

As mentioned already in the Introduction, recent ultraviolet photoemission spectroscopy (UPS) high-resolution ex-

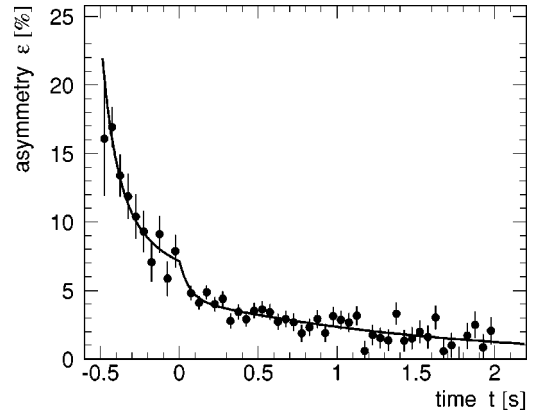


FIG. 2. Observed asymmetry as a function of time for a “hot” hydrogen-covered Si(111) surface. The data are fitted according to Eq. (2) to two relaxation rates using an unpublished code.(Ref. 62)

periments found a narrow parabolic probably adatom-derived band with a bottom about 300 meV below ϵ_F .¹ The electronic origin of this band is not yet clarified completely. A complex interplay of rest atom and adatom dangling bonds seems to contribute. Adsorption on these dangling bonds is a favored interpretation of alkali-metal adsorption experiments (mainly K),^{14,35,36} however, for Li there is a preference for adsorption on the adatom dangling bonds.³⁷ Thus, we expect that nuclear-spin-relaxation experiments on Li adsorbed with very small coverage [10^{-4} and below, that is, one Li atom per 200 unit cells of the (7×7) reconstruction] will probe the electron correlations generating the dispersive band.

While taking T_1 data on Li adsorbed on the clean Si(111)-(7×7) surface, it was flashed every 10 min to about 500 K and every 1–2 h to 1000 K, thus preventing unpolarized ^7Li from accumulating to a considerable fraction on the surface which represents the major part of the atomic beam (Sec. II). In such way 10^{-4} ML of Li at most was accumulated. Figure 3 displays the data for $\alpha = 1/T_1$ as a function of temperature and magnetic-field strength. Part of the 65-mT data has been published previously,² but remeasured at 200 K, 300 K, and 400 K. The data follow a linear temperature dependence quite well which can be characterized by $T_1T = (498 \pm 117) \text{ s K}$. This value is in perfect agreement with the slope of previous data.² They are, moreover, independent of magnetic-field strength in the experimentally accessible range. As shown also previously,² they are independent of doping, which was considered as an indication that the adatom dangling bonds are responsible for the fluctuating electron spins. The data of Fig. 3 exhibit “Korringa relaxation” quite well and may therefore be taken as a sign of the metallicity of the (7×7) reconstruction of the Si(111) surface. However, since the relaxation rates are 1.7 times higher than those found under similar circumstances for ^8Li adsorbed on the metal surface Ru(001) [$T_1T = (852 \pm 131) \text{ s K}$ (Ref. 31)], a more detailed discussion is necessary.

For metals, the main source of electronic nuclear-spin relaxation is caused by Fermi contact interaction of the nuclear-spin with fluctuating electron spins. Since for all realistic situations the electron correlation time is much smaller than the nuclear Larmor period (at 1 T about 2

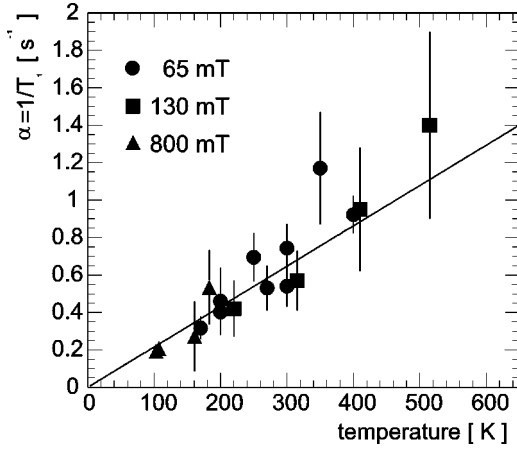


FIG. 3. Nuclear-spin-relaxation rates $\alpha = 1/T_1$ as a function of substrate temperature for three different magnetic fields for ^8Li adsorbed on a clean $\text{Si}(111)-(7\times 7)$ surface. The average Li coverage from the atomic beam was below 10^{-4} ML. The solid line is a fit to the data assuming a linear dependence on surface temperature.

$\times 10^{-7}$ s), the relaxation rate is, as observed, independent of the magnetic-field strength. The necessary mutual spin flip of the nucleus and of the electron can only occur for electrons around the Fermi energy, which explains the linearity of the relaxation rate with surface temperature T . (For further details see Refs. 3–5 and Appendix B.) However, for a “metallic” surface such as that of the (7×7) reconstruction, we cannot expect the description of nuclear-spin-relaxation rates to be based on the interaction of the nuclear-spins with the moments of “free” electrons occupying plane-wave Bloch states [noninteracting electron gas, Eq. (B8) in Appendix B]. Not only does the recently found narrow band around ϵ_F , point to an increased electron localization¹ but so do the already mentioned larger relaxation rates, as compared to those of ^8Li adsorbed on the $\text{Ru}(001)$ metal surface.

For a system as complex as that of low coverage Li adsorption on $\text{Si}(111)-(7\times 7)$, T_1 times are theoretically not yet predictable. We therefore follow arguments here originally developed for similar experiments in liquid semiconductors³⁸ and use the correlation time formalism to derive an approximate analog of the standard expression of relaxation rates for metal electrons described by Bloch wave functions. (For details see Appendix B.) Choosing as correlation time τ_e , the “lifetime of residence” of an electron at the ^8Li site (dangling bond) by means of Eqs. (B5) and (B6), the T_1 time can be expressed as

$$\alpha = \frac{1}{T_1} = \frac{1024\pi^2}{9\hbar} \mu_e^2 \left(\frac{\mu(^8\text{Li})}{I} \right)^2 |\langle |\psi(0)|^2 \rangle|^2 \text{DOS}(\epsilon_F) \cdot \tau_e \cdot \frac{kT}{\hbar}. \quad (3)$$

($|\langle |\psi(0)|^2 \rangle|$ is the probability of finding an electron at the Li nucleus and $\text{DOS}(\epsilon)$ is the density of states.) For metal electrons described by the Bloch wave function, the correlation time approaches [Eq. (B7), Appendix B]

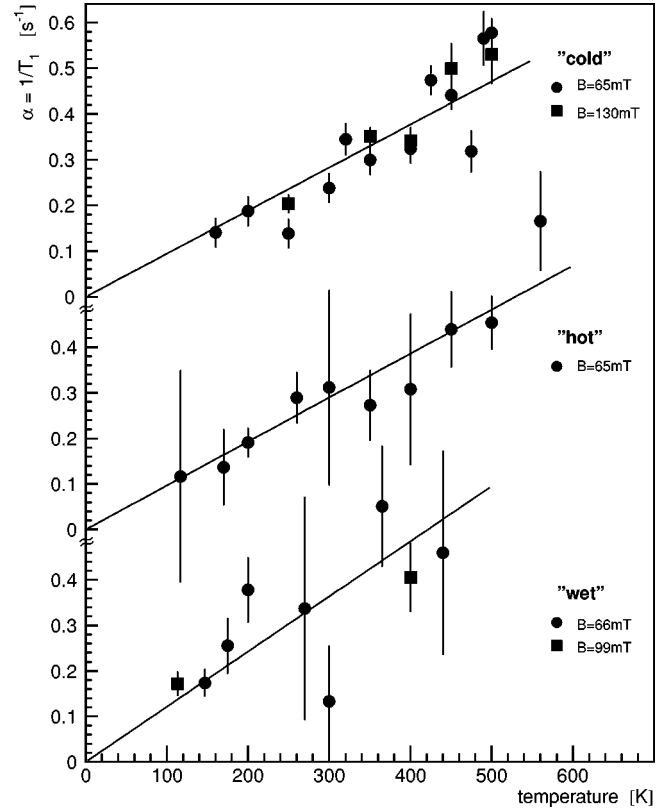


FIG. 4. From top to bottom nuclear-spin-relaxation rates as a function of substrate temperature for Li adsorbed on “cold” and “hot” hydrogen-covered, as well as “wet” chemical hydrogen-terminated $\text{Si}(111)$ surfaces. Various symbols indicate various magnetic fields used. Since the surface could not be flashed every 10 min, the Li coverage was between 10^{-3} and 10^{-2} ML.

$$\tau_e = \hbar \text{DOS}(\epsilon_F) \quad (4)$$

and the resulting expression for $\alpha = 1/T_1$ [Eq. (3)] agrees then within a factor $\pi/4$ with the familiar form for a degenerate noninteracting electron gas [Eq. (B8)]. Thus, an increasing correlation time τ_e , equivalent to an increasing localization, leads to an enhanced nuclear-spin relaxation. This is the basic reason why the relaxation rates for Li adsorbed on $\text{Si}(111)-(7\times 7)$ considerably exceed the one observed for Li adsorption on the metallic $\text{Ru}(001)$ surface.

Three frequencies/time scales enter the description: the precession frequencies of the nuclear and electronic magnetic moments in the external magnetic field B , $\omega_I/B = 3.94 \times 10^7 / (\text{s T})$ and $\omega_e/B = 1.76 \times 10^{11} / (\text{s T})$, respectively, and the electron correlation time τ_e . It follows from the discussion of Eq. (B3) ($\tau = \tau_c$) that the observed magnetic-field independence of the relaxation rates requires $\omega_I \cdot \tau_e \ll 1$. Experimentally, magnetic fields were always lower than 1 T and thus $\tau_e \ll 2.5 \times 10^{-8}$ s, which is generally fulfilled in “metallic” systems (see additionally the discussion below).

The picture drawn “lives” from the electromagnetic fields fluctuating in time, which leads to the electron-nuclear-spin-flip flops and thus to a change of the energy of the spins (magnetic moments) in the external magnetic field. Since the

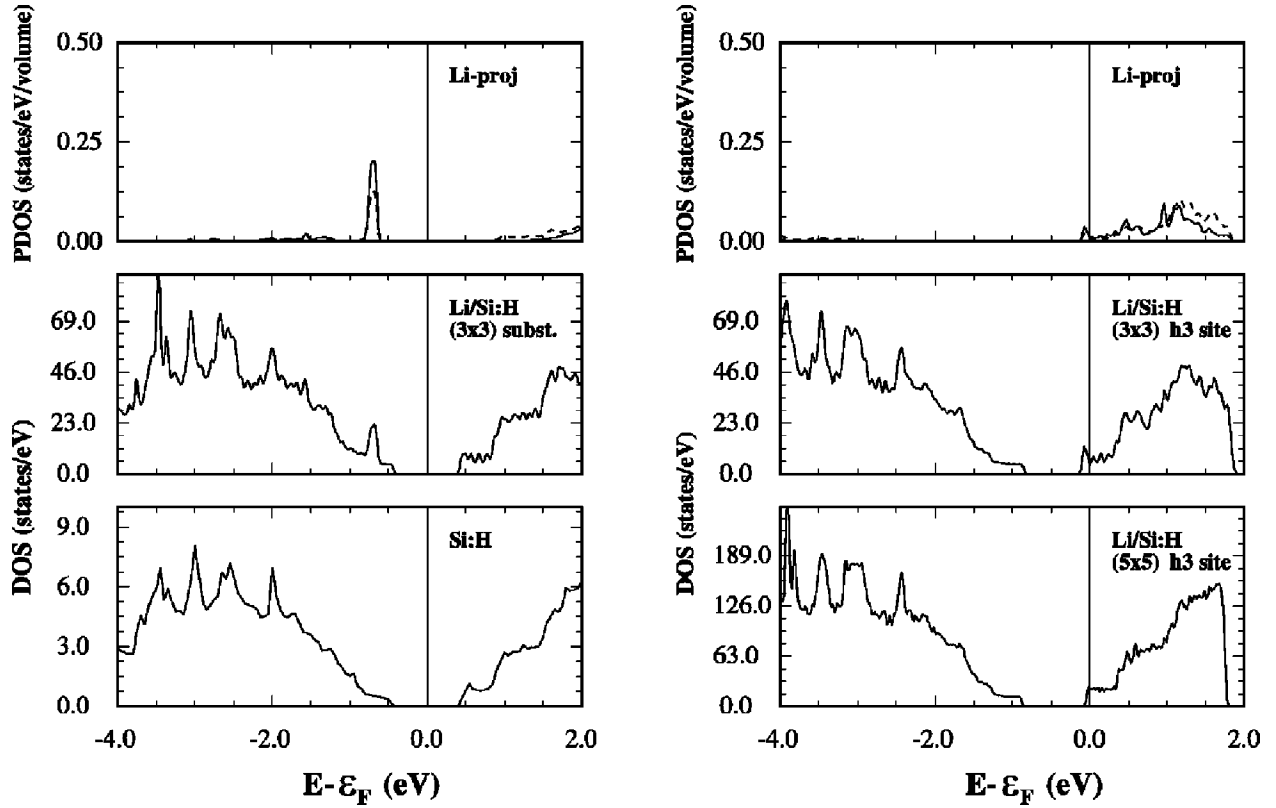


FIG. 5. Density of states from FLAPW calculations for Li adsorbed on a substitutional site (left) and the threefold hollow site h_3 (right). The lower graphs show the results for a perfect hydrogen-terminated surface and the middle one for (5×5) Li adsorption. The upper graph displays the Li projected results, indicating the s -wave part with respect to the Li nucleus by the dashed line.

magnetic moment of the electron is about three orders-of-magnitude larger than the nuclear one, it is dominated by the electronic part. This energy can only be absorbed or emitted by electrons with energies around ϵ_F , since only around the Fermi energy empty states exist. This leads to the linearity of the relaxation rates with temperature [Eq. (B6)].

However, electron-spin flips can occur only if the bandwidth is wide enough to accommodate both electronic spin states.³⁹ [For details see Eq. (11) in Ref. 6.] This leads to the condition

$$\epsilon_F > 2\mu_e B = \hbar\omega_e, \quad (5)$$

which means $\epsilon_F > 0.1$ meV for $B = 1$ T. Furthermore using in Eq. (B7) the approximation $\tau_e \approx \hbar \text{DOS}(\epsilon_F) \approx \hbar/\epsilon_F$ one obtains

$$\tau_e \approx \frac{\hbar}{\epsilon_F} < \frac{\hbar}{\hbar\omega_e} = \frac{1}{\omega_e}, \quad (6)$$

that is,

$$\tau_e \omega_e < 1.$$

For a magnetic field of, e.g., 1 T, the electronic correlation time τ_e has to be shorter than 6×10^{-12} s in order to observe “Korringa relaxation.” For an electronic system the correla-

tion times can obviously be quite large, which means the electrons can be quite localized and “Korringa relaxation” still observable.

Here, it is worthwhile mentioning that on the basis of a Hubbard-like Hamiltonian describing the degenerate electron gas of the adatom dangling bonds, hopping integrals of 25 meV and 75 meV were found leading to a band around the Fermi energy with a width of only 100 meV.^{40,41} This value is considerably smaller than the bandwidth of 300 meV found experimentally.¹ But the correlation times of a few 10^{-14} s associated with such a picture are still short enough for “Korringa relaxation” to occur.

IV. THE HYDROGEN-COVERED AND -TERMINATED Si(111) SURFACES

Figure 4 displays from top to bottom the temperature dependence of relaxation rates $\alpha = 1/T_1$ for Li adsorbed on “cold” and “hot” hydrogen-covered, as well as on “wet” chemically hydrogen-terminated Si(111) surfaces. (Part of the “cold” data has been published previously.²) As samples, modestly n - and p -doped crystals with resistivities between 1 and 100 Ω cm were used. They were prepared and characterized as described in Appendix A. Only the “wet” chemically terminated surfaces were annealed to about 500 K for several minutes after the transfer into the UHV. Since the results do not depend on doping, the data obtained with n - and p -doped samples are not plotted separately.

The major difference in the previous measurements on the clean (7×7) reconstruction is that the hydrogen-covered and -terminated surfaces could not be flashed about every hour to prevent accumulation of unpolarized ^7Li . Otherwise, the adsorbed hydrogen would have desorbed as well. The data points of Fig. 4 were therefore obtained by collecting data over about a day, thus accumulating unpolarized ^7Li of about 10^{-3} – 10^{-2} ML.

Despite adsorption on a real semiconductor the relaxation rates are surprisingly still linear in temperature and magnetic-field independent. They are, however, about a factor of 2 smaller than the ones observed for the (7×7) reconstructed surface. It is a further surprise that for all three kinds of preparation the linear temperature dependence is about the same with $T_1 T \approx 1000$ s K. Discussing these results one should keep in mind that at saturation the “cold” and “hot” hydrogen-covered surfaces are far from being as perfect as the “wet” chemically terminated one.^{8,16} But the almost identical T_1 times found for these Si(111):H surfaces and in particular their agreement with the T_1 times for the almost perfect “wet” chemically hydrogen-terminated Si(111)-(1 \times 1):H surface forces an interpretation which considers the adsorbed Li itself as the source of the fluctuating electron spins (moments) rather than, as for the clean surface, the electronic structure of the surface. Experimental and theoretical investigations on potassium adsorbed at elevated coverages on a “hot” hydrogen-covered and hydrogen-terminated Si(111) surface favor such an interpretation as well.^{14,42,43}

In order to obtain further theoretical insight on the Li adsorption, in particular at low coverages, we performed *ab initio* all-electron full potential linearized augmented plane-wave (FLAPW) calculations following schema described recently.^{44–46} Those calculations are now able to describe semiconductors without further assumptions. In order to save computing time, two adsorption sites were selected for adsorption on the perfectly H-terminated Si(111) surface: a substitutional site, in which the adsorbed Li replaces an adsorbed H atom, and the threefold hollow site h_3 .⁴⁷ The latter turned out to be the energetically favored K adsorption site.^{14,43} (Details of the calculations will be published elsewhere.⁴⁸) Structural optimization with force and total-energy calculations were always performed. The lower graph to the left of Fig. 5 displays the density of states, $\text{DOS}(\epsilon)$, for the perfect hydrogen-terminated Si(111)-(1 \times 1):H surface. A band gap of about 0.85 eV is clearly visible, which is close to the experimentally observed one (about 1.1 eV).^{7,19} The graphs in the middle display the results for the (3×3) adsorption of Li (coverage $\Theta = 0.11$). The left graph is for the substitutional site and the right one for the threefold hollow site h_3 . The results for the substitutional site support the view of the chemical similarity of H and Li: Li on a substitutional site just changes the DOS in the valence band at about 1.4 eV below ϵ_F , as the Li projected $\text{DOS}(\epsilon)$ shows, displayed in the upper panel. The system remains semiconducting with an essentially unchanged band gap. In contrast, adsorbing Li on the threefold hollow site h_3 builds up the $\text{DOS}(\epsilon)$ at the bottom of the conduction band (middle graph on the right), as identified further in the Li projected $\text{DOS}(\epsilon)$ in the upper panel on the right. At this coverage (0.11 ML)

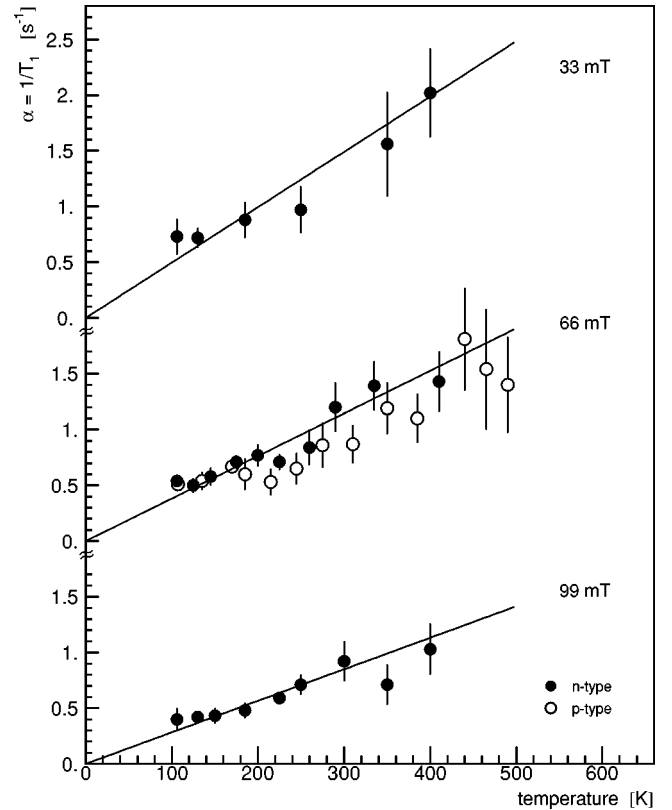


FIG. 6. Nuclear-spin-relaxation rates as a function of substrate temperature and magnetic field for Li adsorbed on an unannealed “wet” chemically hydrogen-terminated Si(111)-(1 \times 1):H surface. Open and full symbols indicate data observed for *n*- and *p*-doped material, respectively. The solid line is a fit to the data assuming a linear dependence on substrate temperature.

the sample becomes metallic since the Fermi energy is moved upon Li adsorption to the bottom of the conduction band. This might also have been expected since Li in bulk silicon is a donor with a binding energy of about 33 meV.^{49,50} Additionally, the lower left panel of the figure displays the result for a (5×5) Li structure for the h_3 adsorption site (coverage $\Theta = 0.04$) which still indicates a metallic sample.

These results are also in accordance with high-resolution electron-energy-loss spectroscopy (HREELS) experiments, which at very low potassium coverage (0.07 of the K saturation coverage) find the formation of a charge accumulation layer (two-dimensional electron gas) at the surface of a hydrogen-terminated Si(111)-(1 \times 1):H crystal.⁹ Since the electrons building up the DOS around ϵ_F are essentially *s* electrons with respect to the Li nucleus, as the Li projected $\text{DOS}(\epsilon)$ shows (upper graph to the right), the local density of states (LDOS) (ϵ_F) will become nonzero and we expect “Korringa-like” relaxation rates linear in temperature for such a sample.

Unfortunately, such calculations cannot be performed for Li coverage of 10^{-3} because of too large a unit cell. However, in order to obtain nevertheless at least a qualitative estimate down to which coverage adsorbed Li might form a band at the bottom of the conduction band, we may follow the arguments on the occurrence of the Mott metal-

semiconductor transition, originally developed for the bulk.^{51–53} For this we recall again that Li is a donor in bulk silicon with an ionization energy of 33 meV. Thus, the donor wave function is quite extended with a Bohr radius of about $a_0 \approx 20 \text{ \AA}$ ($\epsilon = 12$). Lacking other information, we now assume that this radius is also typical for the extension of the Li donor wave function on the hydrogen-covered surface. Then below an averaged Li distance of about $4a_0 \approx 80 \text{ \AA}$ (Mott criterion^{51–53}) the surface should be metallic. This corresponds to a coverage of about 9×10^{-4} . Certainly, at such a low coverage the LDOS(ϵ_F) will be small, but due to the enhancement through the probably long “electron lifetimes of residence” τ_e [Eq. (4)] the relaxation rates are enhanced quite a bit [Eq. (3)].

Temperature-dependent T_1 data on ^8Li adsorbed on the “as-prepared” hydrogen-terminated surface (not annealed) bear another surprise. The data of Fig. 6 display such data for three values of the magnetic fields. Most striking are the large relaxation rates, which not only exceed the ones for the annealed surface considerably (Fig. 4), but also the one for the (7×7) reconstruction at low magnetic field (Fig. 3). They are, moreover, still independent of bulk doping, but rather strongly dependent on magnetic-field strength. They deviate slightly from the strict linear temperature dependence which is indicated by the solid lines. Up to now, in none of our T_1 data on any system has such behavior been observed. As remarked in the Introduction, without annealing we deal probably with an undoped surface with midgap Fermi energy due to hydrogen passivation of both the donors and acceptors.^{19–22} Thus, nuclear-spin relaxation of adsorbed lithium must be caused again by the adsorbed Li itself.

V. OUTLOOK

It was shown that in the short correlation time limit $\omega_l \tau_e \ll 1$, which we only addressed here, nuclear-spin-lattice relaxation rates are proportional to the typical electronic correlation time τ_e (“lifetime of residence”) of the system [Eq. (3)]. They become longer with increasing localization and the relaxation rates increase as long as the associated bandwidth is large enough to accommodate energetically the electron-spin flip [$\epsilon_F > \hbar \omega_e$, Eq. (5)]. For Li adsorption on the (7×7) reconstruction this enhancement of the relaxation rate is counterbalanced by the fact that only a few electrons in the adatom dangling bonds contribute to the DOS(ϵ_F). [Eq. (3); according to Refs. 40 and 41 only two electrons contribute.] Thus, the surprisingly high relaxation rates found for ^8Li adsorbed at very low coverages of around 10^{-4} ML on the (7×7) reconstruction are a delicate balance between these two contributions. A further understanding certainly requires detailed all-electron calculations which are, in principle, now feasible,⁴⁶ certainly not for a coverage of 10^{-4} ML, but maybe for 2×10^{-2} ML, that is, about one adsorbed Li atom per (7×7) unit cell.

The surprisingly preparation-independent relaxation rates for Li adsorbed on hydrogen-covered and -terminated surfaces force an interpretation which considers the adsorbed Li itself as the source of fluctuating electron spins. (Because of experimental reasons, the Li coverages in these experiments

now exceed the 10^{-4} -ML level and reach 10^{-3} – 10^{-2} ML.) The adsorbed Li forms a band and the Fermi energy moves to the bottom of the conduction band. This interpretation is supported by *ab initio* all-electron density approximation calculations. It is further in accordance with recent UPS and HREELS experiments which find even at very low potassium coverages the formation of a two-dimensional electron gas at the surface of hydrogen-covered Si(111) surfaces.^{9,42} Since K and Li may act differently, certainly similar experiments with Li are necessary to decide finally. UPS experiments are underway. First results already confirm our picture, at least for an *n*-doped Si(111) crystal.⁵⁴

ACKNOWLEDGMENTS

We thank Professor Dr. W. W. Warren (Oregon) who introduced us to the rich experimental field of NMR in semiconductors and Professor Dr. A. Pucci (Heidelberg) for their continuous support and for the opportunity to perform the IRTS measurements. This work was supported partly by the Bundesministerium für Bildung und Forschung, Bonn. Finally, we acknowledge the invaluable support of the Max-Planck-Institut für Kernphysik, Heidelberg, at which the experiments were performed.

APPENDIX A

Prior to any preparation of a hydrogen-covered or -terminated surface each sample was cleaned of removable contaminants by rinsing with fresh ultrapure (UP) water (UP water, about 18 MΩ cm), acetone, UP water, methanol, and UP water, again. In contrast to our previous experiments² the native oxide was of high quality, so that it did not have to be removed before wet chemical processing.

A. *In situ* preparation

The samples were outgassed for several hours at 900 K. Then, the oxide was removed by flashes with increasing temperature, finally reaching 1200 K. Preparation of the Si(111)-(7×7) surface (as a starting point) was then performed by Ar⁺-ion sputtering and resistive heating to 1200 K followed by a slow cool down process passing the (“1×1”) ↔ (7×7) phase transition. The resulting surfaces show O and C contamination at or below the detection limit of our Auger electron spectrometer and a sharp LEED pattern.

The easiest method for obtaining a Si(111):H surface is to adsorb atomic hydrogen on a freshly prepared cold (7×7) reconstruction. To do so, H₂ gas (quality 5.8) was dissociated at a hot tungsten filament (2000 K) located 2–4 cm away from the “cold” sample surface kept at 200 K. The hydrogen partial pressure was typically 1×10^{-6} mbar during 150 s, resulting in an approximately H-saturated surface showing a modestly sharp (1×1) LEED pattern. Hydrogen TPD spectra show mono-, di-, and trihydride desorption peaks (Fig. 7 below). Accordingly, as detailed STM studies reveal, a variety of imperfections are still present on these surfaces.^{8,23,55,56}

Polyhydrides, dangling bonds, and structural defects can

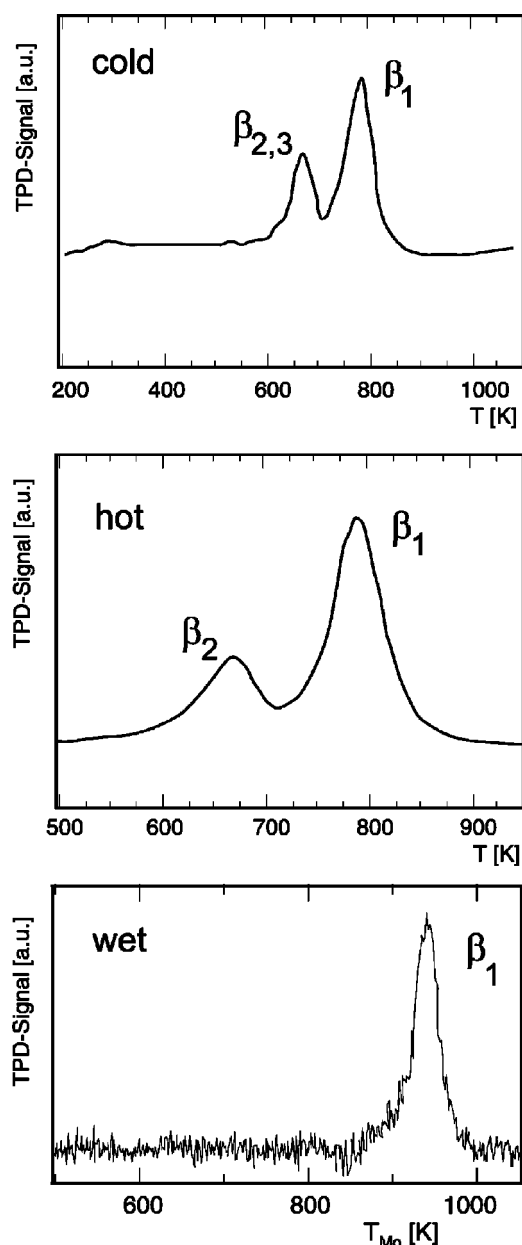


FIG. 7. From top to bottom H_2 TPD spectra of “cold” and “hot” hydrogen-covered and “wet” chemically terminated Si(111) surfaces. The features for mono-, di-, and trihydrides are seen clearly. The TPD spectra for the “wet” chemically hydrogen-terminated Si(111) surface display only the features of a monohydride. They are shifted in desorption temperature since the thermocouple could not be mounted directly on the Si sample itself.

be greatly reduced, exposing a hot surface to a high dose of atomic hydrogen.^{15,16,24} Applying 3000-L H_2 during 150 s to the “hot” (7×7) reconstructed surface at 660 K and a hot filament to dissociate, we obtained a sharp (1×1) LEED pattern and the smallest dihydride to monohydride ratio in the TPD (Fig. 7 below). To better pump the high partial pressure of hydrogen a second turbomolecular pump in line with the UHV turbo pump prevented the H_2 molecules from diffusing back into the UHV.

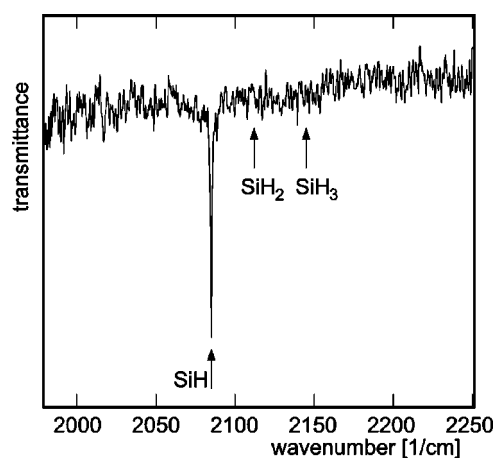


FIG. 8. Infrared transmission spectrum for a “wet” chemically hydrogen-terminated Si(111) surface. Only the Si-H stretch vibration at 2085 cm^{-1} is observed. The vertical lines mark the frequencies at which Si- H_2 (2112 cm^{-1}) and Si- H_3 (2145 cm^{-1}) appear.

B. *Ex situ* preparation

While “cold” *in situ* hydrogen-covered samples still possess stacking faults, “hot” covered ones suffer from stacking faults only to an extent of about 5% of the surface area.¹⁶ However, both the concentration of point defects and the long-range order are still poor, as compared to wet chemically etched Si(111) samples. Therefore, we adopted the method of hydrogen termination in an aqueous solution of ammonium fluoride as described in the literature.^{17,18} The preparation took place under a commercial laminar flow box located near the accelerator facilities in a dust-reduced environment. An accelerator area is a hostile environment to build up such a simple “clean room.” We therefore tried to approach the ideal setup by installing the flow box within a plastic tent close to the UHV chamber, which is connected via the source for polarized ^8Li to the accelerator beam line.

A flat Teflon bowl was used for etching. Afterwards the sample was rinsed with fresh UP water supplied from a commercial desktop unit, (NOWApure select, Fa.KSN-Wassertechnik, Nistertal, Germany). The sample was handled with Al_2O_3 tweezers at its corners. Certain organics (visible in the AES) are hard to detect, monitoring resistivities of about $18\text{ M}\Omega\text{ cm}$. A weak ozone source (UV lamp) was therefore added to the UP water machine to stop organic metabolism. This procedure turned out to be rather effective and as essential as the cleanliness of all instruments.

Within about 60 s after preparation the sample was transferred through the fast load lock system into the vacuum and within about seven minutes into the UHV where each sample was characterized by AES, LEED and TPD. The TPD spectra now showed only the monohydride desorption feature (Fig. 7 below). In AES spectra all contaminants were below the detection limit and LEED displayed a sharp (1×1) pattern.

In order to check our preparation further, the samples had to be transported in a mobile chamber to a UHV infrared (IR) spectroscopy setup and an atomic force microscope. IR spectra showed a monohydride adsorption peak only and no polyhydrides (Fig. 8 below). Atomic force microscopy (not

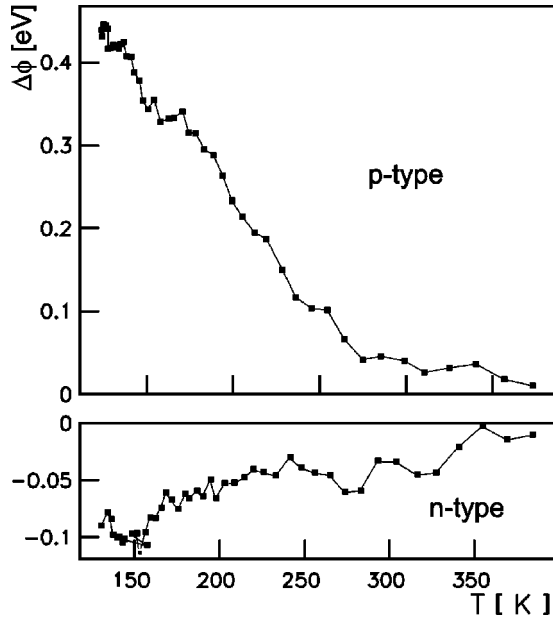


FIG. 9. Temperature-dependent change in work function $\Delta\Phi$ for p - and n -type silicon. $\Delta\Phi = 0$ is arbitrarily chosen at high temperature.

shown) showed monoatomic steps with a terrace width corresponding to the macroscopic miscut of 2000 ± 170 Å.

C. Characterization

Aside from LEED and AES spectra, TPD experiments were mainly used to characterize the hydrogen-covered and -terminated surfaces. Additionally, infrared transmission spectroscopy (IRTS) and an AFM were applied to characterize the terminated surface further. Even though highly desirable, scanning tunneling microscopy (STM) could not be applied because of the already mentioned hostile and strongly vibrating environment of an accelerator laboratory.

Figure 7 displays from top to bottom TPD spectra of desorbing H_2 obtained from a “cold” and a “hot” hydrogen-covered surface as well as from a “wet” hydrogen-terminated one. Both, the “cold” and “hot” covered surfaces show features for mono-, di- and trihydrides at the well-known temperatures. (See Ref. 57, and the discussion therein.) The “hot” covered one displays, however, the lowest di- and tri- to monohydride ratio achievable for *in situ* adsorption of atomic hydrogen. In contrast, the TPD spectrum of the hydrogen-terminated surface displays exclusively the monohydride feature. It is shifted in desorption temperature since for an *ex situ* prepared surface the thermocouple was mounted at the small Mo shuttle of the fast load lock, which did not have a perfect thermal contact to the Si sample.

IRTS was performed at another laboratory at Heidelberg University. For transportation a small bakable vacuum chamber (10^{-6} mbar) was used. Since the IRTS setup is designed for transmission and reflection experiments on thin metal films, the infrared light passed through the sample only once. An IRTS spectrum taken at 130 K is shown as an example in Fig. 8. The light was polarized in the plane of incidence and

hit the crystal at an angle of 60° . Only one sharp absorption line at the position of the Si-H stretch vibration⁵⁸ of 2085 cm^{-1} with a width of 1.25 cm^{-1} full width at half maximum was observed. The width reflects the resolution of the spectrometer setup. No indications of lines at 2112 cm^{-1} or 2145 cm^{-1} at the frequency of the di- or trihydrate stretch vibration were found.⁵⁹

At an ideal Si(111)-(1×1):H surface all dangling bonds are saturated by atomic hydrogen, resulting in a surface free of electronic surface states. The position of the Fermi level is as in the bulk for such a surface. Temperature-induced changes in carrier-concentration shift the bulk Fermi level and should be detectable as changes in work function. The data shown in Fig. 9 were obtained during the cooling phase from samples which had been annealed at 700 K for at least 20 s to remove the near surface passivation of the bulk dopants.²⁰ The upper curve is from a p -type sample ($1\text{--}20 \text{ } \Omega \text{ cm}$) and the lower one from a highly doped n^+ -type sample ($3.3 \times 10^{-3} \text{ } \Omega \text{ cm}$). Changes in work function are 0.45 eV and 0.1 eV for p and n^+ types, respectively, as expected for a perfect hydrogen-terminated Si(111):H surface with an unpinned Fermi level.

APPENDIX B

Since NMR is not a widespread technique in surface science yet, we will briefly summarize a few arguments on spin-lattice relaxation rates for “metalliclike” systems. We follow closely arguments originally developed for similar investigations in liquid semiconductors,³⁸ and of course standard textbooks. (Ref. 3, Chapters I and IX.)

Spin-lattice relaxation is best discussed in terms of time correlation functions for the fluctuating interaction between the electron and nucleus responsible for the relaxation.^{3,4,6} For a random time-dependent perturbation $H'(t)$ the probability for a transition from nuclear-spin sublevel m to m' is given by the standard expression

$$W_{m,m'} = \frac{1}{\hbar^2} \int_{-\infty}^{+\infty} e^{i(m'-m)\omega_I t} \times \overline{\langle m|H'(t)|m'\rangle \langle m'|H'(0)|m\rangle} dt, \quad (\text{B1})$$

where ω_I is the nuclear Larmor frequency and the bar denotes an ensemble average. Since correlation functions can be calculated from first principles in rare cases only,⁶⁰ a common procedure is to approximate them by

$$\overline{\langle m|H'(t)|m'\rangle \langle m'|H'(0)|m\rangle} = \overline{\langle m|H'(0)|m'\rangle}^2 e^{-|t|/\tau}, \quad (\text{B2})$$

where τ is an appropriate correlation time of the fluctuating interaction. Inserting into Eq. (B1) one yields as the transition probability

$$W_{m,m'} = \frac{1}{\hbar^2} \overline{|\langle m|H'(0)|m'\rangle|^2} \frac{2\tau}{1 + [(m'-m)\omega_I\tau]^2}. \quad (\text{B3})$$

For the purpose of this paper we need to consider only the short correlation time limit ($\omega_I \tau \ll 1$, extreme motional narrowing, white spectrum).

We now restrict H' to the most important interaction in/on metallic systems, the Fermi contact between electron and nucleus,

$$H' = \frac{16\pi}{3} \mu_e \left(\frac{\mu(^8\text{Li})}{I} \right) \vec{I} \vec{S} \delta(\vec{r}), \quad (\text{B4})$$

with \vec{I} and \vec{S} the nuclear- and electronic spin operators and \vec{r} the electron coordinate.

Based on the assumption that the incoherence between local fields can be “seen” by two different nuclear-spins, one can express $1/T_1$ in terms of a fictitious $I=1/2$, $S=1/2$ fluctuating matrix element (Ref. 3, p. 362):

$$\alpha = \frac{1}{T_1} = \frac{4}{\hbar^2} \left| \left\langle -\frac{1}{2} \middle| H' \middle| \frac{1}{2} \right\rangle \right|^2 \cdot \tau. \quad (\text{B5})$$

We may identify τ by τ_e which has the significance of a “lifetime of residence” of an electron on a nuclear site.³⁸ Then one obtains finally for the fluctuating matrix elements squared

$$\left| \left\langle -\frac{1}{2} \middle| H' \middle| \frac{1}{2} \right\rangle \right|^2 = \left| \frac{256\pi^2}{9\hbar^2} \mu_e^2 \left(\frac{\mu(^8\text{Li})}{I} \right)^2 \right| \cdot \langle |\Psi(0)|^2 \rangle^2 \cdot \tau_e \cdot \text{DOS}(\epsilon_F) \cdot kT. \quad (\text{B6})$$

The factor $\text{DOS}(\epsilon_F) \cdot kT$ was introduced additionally; it accounts for the effect of energy conservation, which means

that only electrons in an interval of width kT around ϵ_F can contribute to the relaxation process. The quantity $\langle |\Psi(0)|^2 \rangle$ denotes the s -electron probability at the nucleus averaged over all states at the Fermi energy. Combining Eq. (B5) with Eq. (B6) we get the result of Eq. (3) in Sec. III.

Returning now to an “nearly-free-electron gas” the appropriate correlation time is the time τ during which an electron interacts with a particular nucleus. It is roughly the time required for an electron to travel at the Fermi velocity for one nearest-neighbor distance a . For “nearly free electrons” the Fermi velocity v_F is related to $\text{DOS}(\epsilon_F)$, the density of states at ϵ_F , by^{51,61}

$$v_F \approx \frac{2a}{\hbar \text{DOS}(\epsilon_F)},$$

hence

$$\tau_e \approx \frac{a}{v_F} \approx \hbar \text{DOS}(\epsilon_F). \quad (\text{B7})$$

Using this limit for the correlation time we obtain by inserting Eqs. (B6) and (4) into Eq. (B5)

$$\alpha = \frac{1}{T_1} = \frac{1024 \cdot \pi^2}{9\hbar} \mu_e^2 \left[\frac{\mu(^8\text{Li})}{I} \right]^2 \langle |\Psi(0)|^2 \rangle^2 \text{DOS}(E_F)^2 \frac{kT}{\hbar}, \quad (\text{B8})$$

which is, within a factor $\pi/4$, the standard result obtained from a rigorous derivation starting with delocalized electrons described by Bloch functions.³⁻⁶

*Present address: Freie Universität Berlin, Institut für Experimentalphysik, D-14195 Berlin, Germany.

¹R. Losio, K.N. Altmann, and F.J. Himpsel, Phys. Rev. B **61**, 10 845 (2000).

²D. Fick, R. Veith, H.D. Ebinger, H.J. Jänsch, C. Weindel, H. Winnefeld, and J.J. Paggel, Phys. Rev. B **60**, 8783 (1999).

³A. Abragam, *Principles of Nuclear Magnetism* (Oxford University Press, New York, 1978).

⁴C.P. Slichter, *Principles of Magnetic Resonance* (Springer, Berlin, 1996).

⁵G. Schatz and A. Weidinger, *Nuclear Condensed Matter Physics* (Wiley, New York, 1996).

⁶W. Mannstadt and G. Grawert, Phys. Rev. B **52**, 5343 (1995).

⁷W. Mönch, *Semiconductor Surfaces and Interfaces*, Springer Series in Surface Science edited by G. Ertl Vol. 26, (Springer-Verlag, New York, 1993).

⁸J. Boland, Surf. Sci. **244**, 1 (1991).

⁹R. Biagi, L. Rettighieri, U. del Pennino, V. Panella, and P. Dumas, Surf. Sci. **402**, 547 (1998).

¹⁰K. Hricovini, R. Günther, P. Thiry, A. Taleb-Ibrahimi, G. Indlekofer, J.E. Bonnet, P. Dumas, Y. Petroff, X. Blase, X. Zhu, S.G. Louie, Y.J. Chabal, and P.A. Thiry, Phys. Rev. Lett. **70**, 1992 (1993).

¹¹D.R. Alfonso, C. Noguez, D.A. Drabold, and S.E. Ulloa, Phys. Rev. B **54**, 8028 (1996).

¹²H. Lim, K. Cho, I. Park, J.D. Joannopoulos, and E. Kaxiras, Phys. Rev. B **52**, 17 231 (1995).

¹³X. Blase, X. Zhu, and S.G. Louie, Phys. Rev. B **49**, 4973 (1994).

¹⁴R. Saiz-Pardo, R. Rincón, and F. Flores, Appl. Surf. Sci. **92**, 362 (1996).

¹⁵F. Owman and P. Martensson, Surf. Sci. Lett. **303**, L367 (1994).

¹⁶F. Owman and P. Martensson, Surf. Sci. **324**, 211 (1995).

¹⁷G.S. Higashi, Y.J. Chabal, G.W. Trucks, and K. Raghavachari, Appl. Phys. Lett. **56**, 656 (1990).

¹⁸W. Kern, *Handbook of Semiconductor Cleaning Technology* (Noyes, Park Ridge, New York, 1993).

¹⁹W. Mönch, Phys. Status Solidi A **159**, 25 (1997).

²⁰S. Miyazaki, J. Schäfer, J. Ristein, and L. Ley, Appl. Phys. Lett. **68**, 1247 (1996).

²¹S. Miyazaki, J. Schäfer, J. Ristein, and L. Ley, Appl. Surf. Sci. **117/118**, 32 (1997).

²²L. Ley, J. Ristein, J. Schäfer, and S. Miyazaki, J. Vac. Sci. Technol. B **14**, 3008 (1996).

²³K. Mortensen, D.M. Chen, P.J. Bedrossian, J.A. Golovchenko, and F. Besenbacher, Phys. Rev. B **43**, 1816 (1991).

²⁴Y. Morita, K. Miki, and H. Tokumoto, Surf. Sci. **325**, 21 (1995).

²⁵Y.J. Chabal, J.E. Rowe, and D.A. Zwemer, Phys. Rev. Lett. **46**, 600 (1981).

²⁶W. Widdra, M. Detje, H.D. Ebinger, H.J. Jänsch, W. Preyß, H.

- Reich, R. Veith, D. Fick, M. Röckelein, and H.-G. Völk, *Rev. Sci. Instrum.* **66**, 2465 (1995).
- ²⁷H.J. Jänsch, G. Kirchner, O. Köhlert, M. Lisowski, J.J. Paggel, R. Platzer, R. Schillinger, H. Tilsner, C. Weindel, H. Winnefeld, and D. Fick, *Nucl. Instrum. Methods Phys. Res. B* **171**, 537 (2000).
- ²⁸M. Detje, M. Röckelein, W. Preyß, H.D. Ebinger, H.J. Jänsch, H. Reich, R. Veith, W. Widdra, and D. Fick, *J. Vac. Sci. Technol. A* **13**, 2532 (1995).
- ²⁹W. Preyß, H.D. Ebinger, H.J. Jänsch, R. Veith, D. Fick, M. Detje, C. Polenz, and B. Polivka, *Hyperfine Interact.* **110**, 295 (1997).
- ³⁰M. Riehl-Chudoba, U. Memmert, and D. Fick, *Surf. Sci.* **245**, 180 (1991).
- ³¹H.D. Ebinger, H. Arnolds, C. Polenz, B. Polivka, W. Preyß, R. Veith, D. Fick, and H.J. Jänsch, *Surf. Sci.* **412/413**, 586 (1998).
- ³²V. Dyakonov and G. Denninger, *Phys. Rev. B* **46**, 5008 (1992).
- ³³Z.-Z. Gan and P.A. Lee, *Phys. Rev. B* **33**, 3595 (1986).
- ³⁴M.J. Hirsch and D.F. Holcomb, *Phys. Rev. B* **33**, 2520 (1986).
- ³⁵K. Cho and E. Kaxiras, *Surf. Sci.* **396**, L261 (1998).
- ³⁶H.H. Weitering, J. Chen, N.J. DiNardo, and E.W. Plummer, *Phys. Rev. B* **48**, 8119 (1993).
- ³⁷K.D. Brommer, M. Galván, J.A. Dal Pino, and J.D. Joannopoulos, *Surf. Sci.* **314**, 57 (1994).
- ³⁸W.W. Warren, Jr., *Phys. Rev. B* **3**, 3708 (1971).
- ³⁹A. Narath, in *Hyperfine Interactions*, edited by A.J. Freeman and R.B. Frankel (Academic, New York, 1967).
- ⁴⁰F. Flores, A.L. Yeyati, and J. Ortega, *Surf. Rev. Lett.* **4**, 281 (1997).
- ⁴¹J. Ortega, F. Flores, and A.L. Yeyati, *Phys. Rev. B* **58**, 4584 (1998).
- ⁴²C. Grupp and A. Taleb-Ibrahimi, *Surf. Sci.* **408**, 160 (1998).
- ⁴³R. Saiz-Pardo, R. Pérez, F.J. Garcia-Vidal, R. Whittle, and F. Flores, *Surf. Sci.* **426**, 26 (1999).
- ⁴⁴R. Asahi, W. Mannstadt, and A.J. Freeman, *Phys. Rev. B* **59**, 7486 (1999).
- ⁴⁵R. Asahi, Y. Taga, W. Mannstadt, and A.J. Freeman, *Phys. Rev. B* **61**, 7459 (2000).
- ⁴⁶A. Canning, W. Mannstadt, and A.J. Freeman, *Comput. Phys. Commun.* **130**, 233 (2000).
- ⁴⁷A. Vittadini and A. Selloni, *Phys. Rev. Lett.* **75**, 4756 (1995).
- ⁴⁸W. Mannstadt (unpublished).
- ⁴⁹C.S. Fuller and J.A. Ditzenberger, *Phys. Rev.* **91**, 193 (1953).
- ⁵⁰G. Feher, *Phys. Rev.* **114**, 1219 (1959).
- ⁵¹J.M. Ziman, *Principles of the Theory of Solids* (Cambridge University Press, Cambridge, England, 1964).
- ⁵²O. Madelung, *Introduction to Solid-State Theory* (Springer, Berlin, 1978).
- ⁵³N.F. Mott, *Metal-Insulator Transitions*, 2nd ed. (Taylor & Francis, London, 1990).
- ⁵⁴C. Weindel, Ph.D. thesis, Philipps-Universität, Marburg, 2000.
- ⁵⁵J. Boland, *Adv. Phys.* **42**, 129 (1993).
- ⁵⁶J.J. Boland, *J. Phys. Chem.* **95**, 1521 (1991).
- ⁵⁷G.J. Pietsch, *Appl. Phys. A: Mater. Sci. Process.* **A60**, 347 (1995).
- ⁵⁸P. Dumas, Y.J. Chabal, and G.S. Higashi, *Phys. Rev. Lett.* **65**, 1124 (1990).
- ⁵⁹M. Niwano, M. Terashi, and J. Kuge, *Surf. Sci.* **420**, 6 (1999).
- ⁶⁰M. Luban and J.H. Luscombe, *Am. J. Phys.* **67**, 1161 (1999).
- ⁶¹N.W. Ashcroft and N.D. Mermin, *Solid State Physics* (CBS Asia, Philadelphia, 1987).
- ⁶²H. Winnefeld, Ph.D. thesis, Philipps-Universität, Marburg, 2000; <http://archiv.ub.uni-marburg.de/diss/z2001/0076>